

A two-way photonic interface for linking Sr^+ transition at 422 nm to the telecommunications C-band

Thomas A. Wright^{1,*}, Robert J.A. Francis-Jones^{1,2}, Corin B.E. Gawith³, Jonas N. Becker², Patrick M. Ledingham², Peter G.R. Smith³, Joshua Nunn¹, Peter J. Mosley¹, Benjamin Brecht², and Ian A. Walmsley²

¹*Centre for Photonics and Photonic Materials, Department of Physics, University of Bath, Bath, BA2 7AY, UK*

²*Clarendon Laboratory, University of Oxford, Parks Road, Oxford, OX1 3PU, UK and*

³*Optoelectronics Research Centre, University of Southampton, Southampton, SO17 1BJ, UK*

(Dated: October 16, 2018)

We report a single-stage bi-directional interface capable of linking Sr^+ trapped ion qubits in a long-distance quantum network. Our interface converts photons between the Sr^+ emission wavelength at 422 nm and the telecoms C-band to enable low-loss transmission over optical fiber. We have achieved both up- and down-conversion at the single photon level with efficiencies of 9.4% and 1.1% respectively. Furthermore we demonstrate noise levels that are low enough to allow for genuine quantum operation in the future.

INTRODUCTION

Large scale quantum networks suitable for long-distance secure communication and distributed computation require not only that quantum information may be manipulated reliably, but also communicated successfully between remote nodes [1, 2]. However, existing quantum information processing platforms are not individually able to fulfil both of these requirements. For example, photons can distribute quantum information through fiber networks [3] or via satellite [4] but multi-photon gates remain challenging, whereas trapped ions have achieved high-fidelity two-qubit operations [5] but are unsuitable for sharing entanglement beyond a single laboratory. However, integrating disparate technologies to form a hybrid light-matter quantum network promises the capability to carry out entanglement distribution and quantum communication over long distances [6, 7].

The optical communication bus between nodes must overcome two technical challenges: compatibility between devices operating at different optical frequencies and low loss across large separations. Quantum frequency conversion (QFC), where a photon is coherently shifted to a different frequency band, addresses this difficulty by linking wavelengths as short as the ultraviolet (UV), where many convenient ion transitions are located, and the infrared (IR) telecommunications bands, enabling long-distance low-loss transmission in optical fiber [8].

A diverse range of platforms have been utilized to demonstrate frequency conversion via three- or four-wave mixing, including nonlinear crystals [9, 10], planar waveguides [11, 12], optical fibers [13, 14], microresonators [15, 16] and atomic systems [17, 18]. QFC experiments initially focused on enhancing detection of IR photons by mapping them to the visible and near-infrared (NIR) where efficient silicon photon detectors existed [9, 19]. QFC has since been shown to achieve the frequency remapping of both squeezed light [20, 21] and entan-

gled states [12, 22]. The enhancement offered by QFC to optical interconnects within a quantum network has led to a demonstration of direct coupling between dissimilar quantum memories [23], as well as a multitude of experiments translating node-compatible photons both from [12, 20, 24–30] and to [22, 31–40] different telecommunication bands.

Near-unit efficiency frequency conversion has been demonstrated [14], although, in practice, complexities arising from photon bandwidth, pump induced noise and the required frequency shift have limited the capability of many converters, proving arduous challenges to overcome. QFC via three-wave mixing, in particular, imposes the strict requirement that the high nonlinear coupling be provided by a singular strong pump which additionally must account for the energy difference between the input and target wavelength. In large part, existing QFC experiments have exploited opportune laser wavelengths and transitions predominantly in the red and NIR. The large frequency separation between IR and the blue - UV makes connecting most ion traps to the telecom bands particularly challenging, leading to the proposition of a two stage approach [41]. Classical generation of UV light by means of parametric three-wave mixing is in itself difficult, so far being realized by SHG [42] and sum frequency generation (SFG) [43]. Recently however, developments in the translation of quantum states between ultraviolet and the O-band has been shown [44, 45], albeit only in one direction. The majority of reported conversions thus far have been unidirectional with limited exceptions [46], whereas to create a functional quantum network in fiber, shifting to the telecoms is critical and two-way conversion is desirable.

We report the realization of single-stage bi-directional frequency conversion at the single photon level for interfacing the $S_{1/2} \rightarrow P_{1/2}$ transition in trapped Sr^+ ion qubits (422 nm) with the telecommunication C-band (1550 nm). The conversion is achieved in a magnesium-doped periodically poled lithium niobate (MgO:PPLN) crystal, where $\chi^{(2)}$ sum or difference frequency genera-

tion (SFG or DFG) can be used to achieve up or down conversion of an input photon. By monitoring the conversion of weak coherent light with single-photon detectors, we demonstrate that the noise level, expressed as the actual noise photons normalized to the conversion efficiency, μ_1 [47], is as low as 0.0185 – far below the level required for use as the interface in a hybrid quantum network. This is to our knowledge the only bi-directional link between blue ion transitions and the C-band.

TECHNICAL DETAILS

In order to map the input to the target output wavelength, a strong pump field must be tuned to fulfill the energy conservation requirement $\hbar\omega_{\text{in}} + \hbar\omega_{\text{pump}} = \hbar\omega_{\text{out}}$ for SFG up conversion and $\hbar\omega_{\text{in}} - \hbar\omega_{\text{pump}} = \hbar\omega_{\text{out}}$ for DFG down conversion. In both SFG and DFG the amplitude of the strong pump serves to drive the nonlinear optical response facilitating the conversion. The efficiency of the process is related to the strength of the coupling between the fields in the QFC Hamiltonian:

$$\hat{\mathcal{H}} = i\hbar\kappa A_{\text{pump}}(\hat{a}_{\text{out}}^\dagger \hat{a}_{\text{in}} - h.c.) \quad (1)$$

determined by the parameter κ , which itself is dependent on the magnitude of the fields but also on their relative phase, spatial overlap in the crystal and a the intrinsic nonlinearity of the material [8].

For such widely separated wavelengths, the large wave-vector mismatch Δk between the propagation constants of the three fields means that phase matching is difficult to satisfy in commonly-available materials. Even typical quasi phase-matched (QPM) crystals that achieve efficient conversion when

$$\Delta k - \frac{2\pi}{\Lambda} = k_{\text{out}} - k_{\text{in}} - k_{\text{pump}} - \frac{2\pi}{\Lambda} = 0 \quad (2)$$

have a poling pitch Λ that is too long to compensate the large Δk in our interaction. Hence, we used a MgO:PPLN crystal fabricated in collaboration with Covision Ltd with ferroelectric domains created using a proprietary electric field poling technique to produce a very short pitch, shown in Fig. 1. A photoresist pattern was created on the $-z$ (bottom) face of a 0.5 mm-thick single-domain z -cut 3 inch diameter MgO:LiNbO₃ crystal wafer. Liquid electrodes were applied to both the patterned $-z$ and unpatterned $+z$ surfaces of the crystal to enable electrical contact with the wafer surface. Domain inversion along the z -axis was performed at room temperature by voltage-controlled application of electric field based on a first stage of domain nucleation above the coercive field of the crystal, and a second stage of domain spreading near the coercive field ($\sim 4.5 \text{ kV mm}^{-1}$); this technique results in inverted domains that traverse the entire thickness of the crystal. The MgO:PPLN wafer

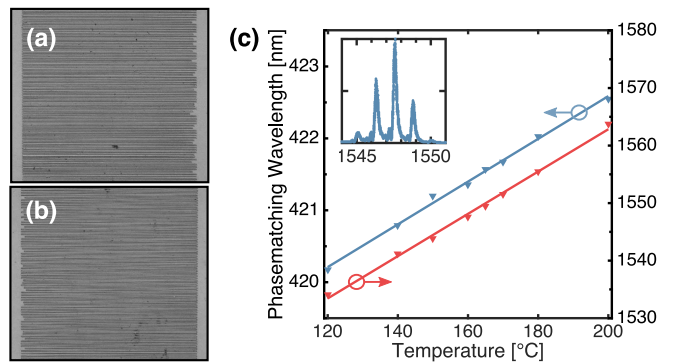


FIG. 1. Optical micrographs of the (a) $+z$ (top) and (b) $-z$ (bottom) surface of one of the $3.75 \mu\text{m}$ periodically poled MgO:LiNbO₃ crystals. (c) Phase-matching characteristics. The temperature response of the phase-matching of the $3.75 \mu\text{m}$ poled crystal, i.e., the wavelength of perfect phase matching as a function of crystal temperature. *Inset* SFG phase-matching curve, i.e., short wavelength output power as a function of input telecom wavelength at constant crystal temperature and pump power.

was diced and polished into multiple chips, each containing five $300 \mu\text{m}$ -wide gratings with periods of 3.75 , 3.85 , 3.95 , 4.05 , and $4.15 \mu\text{m}$ respectively. These periods were calculated to enable SFG and DFG processes between 422 nm and the telecoms C-band. The MgO:PPLN crystal used in this experiment was 19.97 mm long, with the $3.75 \mu\text{m}$ grating selected; it was not anti-reflection coated.

EXPERIMENTAL DEMONSTRATION

Phase-matching characterization

The experimental setup for characterizing the SFG up-conversion is shown in Fig. 2(a). An 80 MHz synchronously pumped tunable dye laser operating at 580 nm wavelength and 30 ps pulse duration (Sirah Gropius) was used to pump the conversion and a tunable continuous-wave (CW) laser with a 40 MHz linewidth (Santec TSL-510 C), provided a coherent IR input that was attenuated to low mean photon number. The pump and input beam size and polarization were set using telescopes, polarizing beam splitters (PBSs), and half-wave plates (HWP) before the beams were combined at a dichroic mirror (DM) and directed towards the MgO:PPLN crystal. A pair of fused silica lenses were then used to focus the overlapped beams into the crystal. Care was taken to balance matching the Rayleigh length of each beam to half the crystal length while minimizing the difference between the cross-sections of the beam waists. Following the crystal, a flipper mirror allowed for the input and pump powers transmitted through the crystal to be measured. The pump, unconverted IR input light and successfully converted violet output were

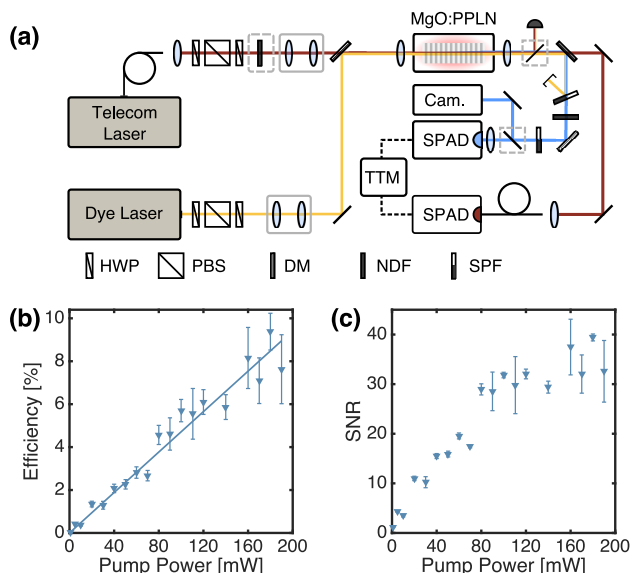


FIG. 2. (a) Experimental setup of the SFG up conversion. (b) Up conversion efficiency of the interface. (c) Signal-to-noise ratio of the up conversion.

then separated using a series of dichroic and short pass (SPF) filters before being directed to two single-photon avalanche diodes (SPADs). At the short wavelength, the pump light was removed using short pass filters at 500 nm and 440 nm as well as a short-pass dichroic filter with an edge at 500 nm. The remaining signal was monitored by a blue-enhanced Si SPAD with a detection efficiency, dead time and dark count rate of 86 %, 43 ns and 6 Hz. For the long wavelength we utilized a fiber-coupled In-GaAs SPAD operating at 9.5 % detection efficiency with a dead time of 10 μ s. A time-tagging module (TTM) was used to record counts from the detectors. A spectrograph with electron-multiplying CCD camera was available to monitor the spectra of the violet light.

In order to maximize the coupling constant, κ , the phase matching of the crystal was first characterized. With the temperature of the crystal stabilized at 160°C, the input IR beam was swept in wavelength whilst the intensity of the converted violet light was measured, mapping out the phase matching curve, for a pump wavelength of 579.6 nm. We observed several distinct peaks in the phase-matching (see Fig. 1), indicative of either multiple frequency modes within the pump beam or inhomogeneous poling across the length of the crystal.

We measured the change in position of the central phase matching peak as a function of temperature, for a range of crystal temperatures by sweeping the input wavelength whilst measuring the output violet power using an amplified photodiode. For the input IR light we measured a temperature response of $\Delta\lambda_{in}/\Delta T = 0.4$ nm/K, corresponding to a change in the output wavelength of $\Delta\lambda_{out}/\Delta T = 0.0297$ nm/K.

Frequency up-conversion

Having established the phase matching response of the crystal, we investigated the achievable up conversion efficiency. IR light at 1547.6 nm was converted to 421.7 nm by pumping the process at 579.6 nm with a fixed crystal oven temperature of 160°C.

We present the external efficiency, η_{ext} , of the SFG conversion in Fig. 2(b), which we define as the mean number of converted photons per second leaving the crystal divided by the number of input photons per second incident and temporally overlapped with the pump. The number of input photons per second, $\langle n \rangle_{in}$, is therefore given by

$$\langle n \rangle_{in} = \frac{P_{in}D}{\hbar\omega_{in}}, \quad (3)$$

where P_{in} was the IR power transmitted through the crystal measured with the pump beam blocked. Due to observations of drift in the IR input power, this was measured both before and after each integration over which we recorded detector counts and used to calibrate the continuous monitoring of the IR light at SPAD detector 2. Due to the CW nature of the input light, the duty cycle D was defined as the pump pulse width multiplied by the repetition rate: $D = \tau_{pump} \cdot R_p$.

The conversion efficiency was then calculated as

$$\eta_{ext} = \frac{S - N}{\langle n \rangle_{in} \eta_{loss}}, \quad (4)$$

where η_{loss} incorporates the detector efficiency (86 %), transmission through optical components (96 %) and, at higher powers, a neutral density filter (NDF) with approximately 20 % transmission used to prevent detector saturation. S and N are the signal and noise counts per second respectively. As the SPAD detectors output only a single click when one or more photons arrive within their dead time, S and N were corrected relative to the measured rates S_{raw} and N_{raw} as follows:

$$S = \frac{S_{raw}}{1 - S_{raw}T_D}; \quad N = \frac{N_{raw}}{1 - N_{raw}T_D}, \quad (5)$$

where $T_D \gg 1/R_p$ is the dead time of the detector. The background noise was measured by blocking the IR input and recording counts at the visible detector with the pump unblocked.

In order to demonstrate the capability of the interface to operate at low photon numbers we set a target input of overlapping an average of two IR photons from the IR attenuated coherent source with every pump pulse. The resulting conversion efficiency is shown in Figure 2(b). The highest measured external efficiency of $\eta_{ext} = 9.4 \pm 0.86$ % was observed for an average pump power of 180 mW. Each point in Figure 2(b) corresponds to a measurement consisting of between 5 and 10 s of integration, beyond which we observed a drop in efficiency. This

was later realized to be due to absorption of the pump light causing localized heating of the crystal, resulting in a change in the phase matching. The phenomenon of pump-power-induced change in Δk for $\chi^{(2)}$ QFC processes has been discussed previously [45, 48]. Additional change in the phase mismatch is also introduced due to the photorefractive effect and as such, when operating over extended periods of time as would be required in a network, the process would be pumped at a constant power, with the phase matching temperature tuning being optimized at the selected pump power. Figure 2(c) shows the signal to noise ratio (SNR) achieved across a range of pump powers, where we define $\text{SNR} = S/N$. The SNR achieved for the point at which we achieved highest conversion was 39.4 ± 0.69 .

Frequency down-conversion

In order to demonstrate a two way interface, we similarly characterized the reverse process, converting single-photon level violet light to IR via DFG. Figure 3(a) shows the modified experimental setup. The input light at 425.5 nm was obtained by second harmonic generation of a 80 MHz repetition rate Ti:sapphire laser operating at 851 nm wavelength and 300 ps pulse duration (Spectra Physics Tsunami) which was synchronized to the clock signal of the dye laser system via active cavity-length control. Replicating the interface between 421.7 nm and the C-band was not possible due to the phase matching restriction of the SHG crystal. In order to successfully translate the violet light to the telecoms C band we tuned the wavelength of the dye laser to 585 nm and adjusted the crystal oven temperature to 226.4°C. This enabled us to optimize conversion to 1560.6 nm. Mitigation of the pump induced change in Δk was achieved by optimizing the oven temperature whilst pumping the nonlinear conversion with an average power of 60 mW, half of the available range. In the long wavelength detection arm the filtering consisted of two long pass filters with edges at 950 and 650 nm. A 8.9 nm-wide band pass filter (BPF) was used, centered at 1570 nm and rotated in order to shift the transmission to accommodate the converted light at 1560 nm.

In Fig. 3(b) we present the external efficiency of the conversion, where we have accounted for sources of loss outside the crystal, as described by Eq. 3. We evaluated η_{loss} , incorporating the detector efficiency ($\sim 9.5\%$), transmission through optical components ($\sim 73\%$) and fiber coupling efficiency ($\sim 65\%$). The duty cycle D was defined as the ratio of the pump and input pulse durations: $D = \tau_{\text{pump}}/\tau_{\text{input}}$. The same target input photon number as the SFG conversion, of $\langle n \rangle_{\text{in}} = 2$ per pulse, was used in the DFG experiment. Across the data collected, counts were measured for integration times longer than 15 s.

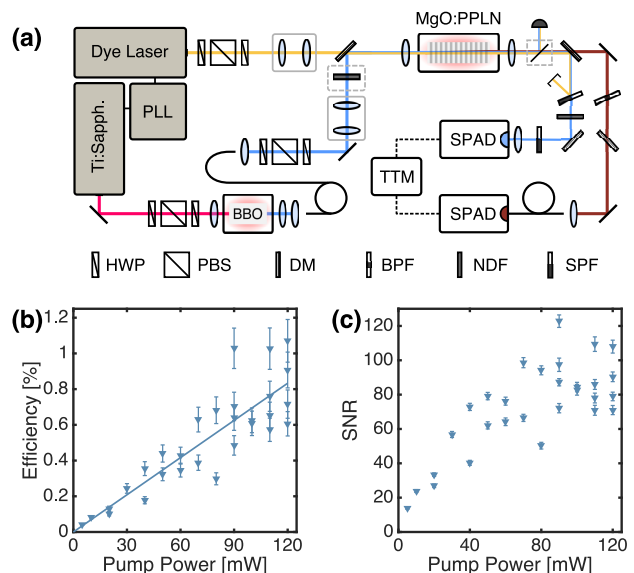


FIG. 3. (a) Experimental setup of the DFG down conversion. PLL: phase-locked loop (b) Down-conversion efficiency of the interface. (c) Signal-to-noise ratio of the down conversion.

The pump and input beam were steered using mirrors ahead of the crystal to optimize the beam overlap leading to a wide distribution of observed conversion at comparable pump powers. A maximum external conversion efficiency of $(1.1 \pm 0.12)\%$ was achieved for a pump power of 120 mW, While significantly lower than the $\sim 6\%$ external efficiency observed for the SFG at equal pump power, the observed value may be partly explained by a change in beam waist between the two experiments. The beam waist of the pump in both experiments was $\sim 43.2 \mu\text{m}$, while the input light beam waist was increased from $\sim 63.3 \mu\text{m}$ in the SFG up conversion to $\sim 112 \mu\text{m}$ in the DFG down conversion. This would indicate that the maximum proportion of the input overlapped by the pump changed from $\sim 46.6\%$ to $\sim 14.9\%$. It could be expected that further optimization of optics selection may yield improved conversion efficiencies, in particular when considered for the DFG down-conversion. Again, we draw attention to the conversion efficiency being limited by the available pump power in the experiment, as can be seen from the linear slope of the efficiency vs pump power curve in Fig. 3(b). The down conversion was shown to be low noise in operation, with a SNR of 108 ± 3.8 measured at the point of highest conversion.

DISCUSSION

Noise analysis

In order to demonstrate that our device is capable of operating as a QFC interface in a quantum network, for

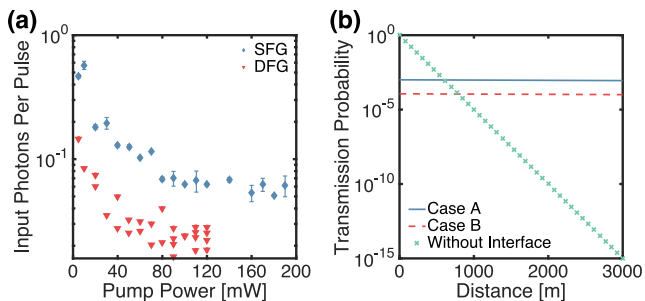


FIG. 4. (a) μ_1 , The lowest number of photons per pulse possible to send into the device to get an $\text{SNR} \geq 1$. (b) Probability of successful transmission of two photons from remote trapped Sr^+ ion processing nodes to an entangler along a fiber network with and without our interface.

both up and down conversion, we calculated the mean input photon number per pulse that would yield a $\text{SNR} = 1$, commonly referred to as μ_1 [47]. Originally defined for quantum memories, the parameter μ_1 provides a useful performance benchmark for frequency conversion as it normalizes the noise by the conversion efficiency, thus precluding noise reduction by pumping with unrealistically low power. The calculated values are shown in Figure 4(a). For the up conversion we found the minimum $\mu_1 = 0.05074$ when operating at a pump power of 180 mW. We note that this value was limited by the pump power in the experiment, as can be seen from the linear slope of the efficiency vs pump power curve, and that these values are obtained without narrow-band spectral filtering. For the down conversion, we find $\mu_1 = 0.0185$ at a pump power of 120 mW.

The very low value of μ_1 for down conversion shows that noise originating from broadband, unphase-matched spontaneous parametric down conversion (SPDC) of the pump field – typically a limiting factor in $\chi^{(2)}$ QFC schemes linking short to long wavelengths [49] – does not inhibit the capability of our system to operate at the single-photon level. As a result, we believe that up converted SPDC, which has been shown to contribute broadband noise to frequency conversion [45, 50], is not the dominant noise source in our SFG configuration. We attribute the contrast in SNR between down conversion and up conversion primarily to the difference in detector sensitivity at the pump wavelength: the Si visible detector is sensitive to the pump wavelength whereas the InGaAs IR detector is not. The resulting inability to detect pump light leaking through the filters during down conversion and commensurate lower noise level suggests that pump leakage is the dominant source of noise in the up conversion configuration. This could in principle be removed by increasing the optical depth of the filters at the pump wavelength.

Our values of $\mu_1 \ll 1$ demonstrate that low-noise operation is possible without narrow-band spectral filter-

ing. Although high-efficiency conversion of nanosecond-duration photons from Sr^+ ions would require increased pulse energy, due to the broadband nature of the noise and its linear dependence on pulse energy we expect that low-noise conversion could be maintained through narrow band filtering as seen in [36, 39]. To illustrate, we consider our device operation in ion compatible down-conversion, utilizing 1 μs duration pump pulses. In our current configuration we observe 3.9×10^{-6} noise photons per 300 ps pump pulse, at the point of highest conversion. Increasing pulse duration to 1 μs would see this number increase by a factor of ~ 3300 . However, replacing our existing 8.9 nm band pass filter at 1570 nm with a 200 MHz filter, similar to that used in [36] would see a reduction of broadband noise by a factor of ~ 5400 , hence maintaining a similar noise contribution overall.

Projected network enhancement

In Figure 4(b) we consider the end-to-end efficiency of three scenarios in which entanglement needs to be established between remote processing nodes, taking into account the transmission loss of fiber at the wavelengths 422 nm and 1550 nm (< 50 dB/km for SM400 at 422 nm and < 0.18 dB/km for SMF-28 at 1550 nm). In case A a violet photon from node 1 is down-converted via our interface and transmitted through a length of optical fiber before reaching the location of the second node, where it is up-converted to allow interference with a photon emitted directly from the node 2. In case B both photons emitted by the ion traps are down-converted before being transmitted through optical fiber and interfered at some midway position. The final case is where no interface is used and a violet photon is emitted from one of the nodes before being transmitted through fiber to the second node whereupon an entanglement link is established. For each case we present the probability of the photons successfully reaching their destination, assuming no coupling loss. We see that the use of our interface would drastically increase the probability of successful end-to-end transmission for remote nodes linked by fiber, even for typical intra-city distances of a few kilometres.

CONCLUSION

We have implemented an interface capable of low noise up- and down-conversion of single-photon-level light with efficiencies of 9.4 % and 1.1 % respectively in a custom-poled MgO:PPLN crystal. When considering the transmission loss of single mode fiber at the Sr^+ emission wavelength of 422 nm relative to that at 1550 nm, our interface would increase the probability of successful transmission of quantum information by 47 orders of magnitude over a distance of 10 km. We have demonstrated

that the noise introduced when converting a weak coherent state is far below the level required to achieve high-fidelity operation with single photons emitted by trapped Sr^+ ions. Hence we believe that our interface will enable long-distance entanglement distribution through chains of nodes containing trapped Sr^+ ions, paving the way to the construction of large-scale quantum networks.

ACKNOWLEDGEMENTS

This work was funded by the UK EPSRC Quantum Technology Hub Networked Quantum Information Technologies, grant number EP/M013243/1. B.B. acknowledges funding from the European Union (EU) Horizon 2020 Research and Innovation Program under Grant No. 665148. P.M.L. acknowledges funding from the European Union Horizon 2020 Research and Innovation Framework Programme Marie Curie individual fellowship, Grant No. 705278.

* t.wright@bath.ac.uk

- [1] H. J. Kimble, *Nature* **453**, 1023 (2008).
- [2] L. M. Duan, M. D. Lukin, J. I. Cirac, and P. Zoller, *Nature* **414**, 413 EP (2001).
- [3] Q.-C. Sun, Y.-F. Jiang, Y.-L. Mao, L.-X. You, W. Zhang, W.-J. Zhang, X. Jiang, T.-Y. Chen, H. Li, Y.-D. Huang, X.-F. Chen, Z. Wang, J. Fan, Q. Zhang, and J.-W. Pan, *Optica* **4**, 1214 (2017).
- [4] J. Yin, Y. Cao, Y.-H. Li, J.-G. Ren, S.-K. Liao, L. Zhang, W.-Q. Cai, W.-Y. Liu, B. Li, H. Dai, M. Li, Y.-M. Huang, L. Deng, L. Li, Q. Zhang, N.-L. Liu, Y.-A. Chen, C.-Y. Lu, R. Shu, C.-Z. Peng, J.-Y. Wang, and J.-W. Pan, *Physical Review Letters* **119**, 200501 (2017).
- [5] C. J. Ballance, T. P. Harty, N. M. Linke, M. A. Sepiol, and D. M. Lucas, *Physical Review Letters* **117**, 060504 (2016).
- [6] I. A. Walmsley and J. Nunn, *Phys. Rev. Applied* **6**, 040001 (2016).
- [7] R. Nigmatullin, C. J. Ballance, N. d. Beaudrap, and S. C. Benjamin, *New Journal of Physics* **18**, 103028 (2016).
- [8] P. Kumar, *Optics letters* **15**, 1476 (1990).
- [9] M. A. Albota and F. N. C. Wong, *Optics letters* **29**, 1449 (2004).
- [10] A. Sambrowski, C. E. Vollmer, C. Baune, J. Fiurásek, and R. Schnabel, *Optics letters* **39**, 2979 (2014).
- [11] C. Langrock, E. Diamanti, R. V. Roussev, Y. Yamamoto, M. M. Fejer, and H. Takesue, *Optics letters* **30**, 1725 (2005).
- [12] S. Tanzilli, W. Tittel, M. Halder, O. Alibart, P. Baldi, N. Gisin, and H. Zbinden, *Nature* **437**, 116 EP (2005).
- [13] H. J. McGuinness, M. G. Raymer, C. J. McKinstrie, and S. Radic, *Physical Review Letters* **105**, 093604 (2010).
- [14] A. S. Clark, B. J. Eggleton, C. Xiong, M. J. Collins, and S. Shahnia, *Optics letters* **38**, 947 (2013).
- [15] Q. Li, M. Davanco, and K. Srinivasan, *Nature Photonics* **10**, 406 (2016).
- [16] X. Guo, C.-L. Zou, H. Jung, and H. X. Tang, *Physical Review Letters* **117**, 123902 (2016).
- [17] A. G. Radnaev, Y. O. Dudin, R. Zhao, H. H. Jen, S. D. Jenkins, A. Kuzmich, and T. A. B. Kennedy, *Nature Physics* **6**, 894 (2010).
- [18] P. J. Bustard, D. G. England, K. Heshami, C. Kupchak, and B. J. Sussman, *Physical Review A* **95**, 053816 (2017).
- [19] A. P. Vandevender and P. G. Kwiat, *Journal of Modern Optics* **51**, 1433 (2004).
- [20] C. E. Vollmer, C. Baune, A. Sambrowski, T. Eberle, V. Händchen, J. Fiurásek, and R. Schnabel, *Physical Review Letters* **112**, 073602 (2014).
- [21] D. Kong, Z. Li, S. Wang, X. Wang, and Y. Li, *Optics express* **22**, 24192 (2014).
- [22] R. Ikuta, Y. Kusaka, T. Kitano, H. Kato, T. Yamamoto, M. Koashi, and N. Imoto, *Nature Communications* **2**, 537 (2011).
- [23] N. Maring, P. Farrera, K. Kutluer, M. Mazzer, G. Heinze, and H. de Riedmatten, *Nature* **551**, 485 (2017).
- [24] A. P. Vandevender and P. G. Kwiat, *JOSA B* **24**, 295 (2007).
- [25] T. Honjo, H. Takesue, H. Kamada, Y. Nishida, O. Tadanaga, M. Asobe, and K. Inoue, *Optics express* **15**, 13957 (2007).
- [26] M. T. Rakher, L. Ma, O. Slattery, X. Tang, and K. Srinivasan, *Nature Photonics* **4**, 786 EP (2010).
- [27] M. T. Rakher, L. Ma, M. Davanco, O. Slattery, X. Tang, and K. Srinivasan, *Physical Review Letters* **107**, 083602 (2011).
- [28] N. Maring, K. Kutluer, J. Cohen, M. Cristiani, M. Mazzer, P. M. Ledingham, and H. d. Riedmatten, *New Journal of Physics* **16**, 113021 (2014).
- [29] C. Baune, J. Griesmer, S. Kocsis, C. E. Vollmer, P. Zell, J. Fiurásek, and R. Schnabel, *Physical Review A* **93**, 010302 (2016).
- [30] M. Allgaier, V. Ansari, L. Sansoni, C. Eigner, V. Quiring, R. Ricken, G. Harder, B. Brecht, and C. Silberhorn, *Nature Communications* **8** (2017).
- [31] H. Takesue, *Physical Review A* **82**, 013833 (2010).
- [32] S. Zasse, A. Lenhard, C. A. Kessler, J. Kettler, C. Hepp, C. Arend, R. Albrecht, W.-M. Schulz, M. Jetter, P. Michler, and C. Becher, *Physical Review Letters* **109**, 147405 (2012).
- [33] K. De Greve, L. Yu, P. L. McMahon, J. S. Pelc, C. M. Natarajan, N. Y. Kim, E. Abe, S. Maier, C. Schneider, M. Kamp, S. Höfling, R. H. Hadfield, A. Forchel, M. M. Fejer, and Y. Yamamoto, *Nature* **491**, 421 EP (2012).
- [34] J. S. Pelc, L. Yu, K. De Greve, P. L. McMahon, C. M. Natarajan, V. Esfandyarpour, S. Maier, C. Schneider, M. Kamp, S. Höfling, R. H. Hadfield, A. Forchel, Y. Yamamoto, and M. M. Fejer, *Optics express* **20**, 27510 (2012).
- [35] B. Albrecht, P. Farrera, X. Fernandez-Gonzalvo, M. Cristiani, and H. de Riedmatten, *Nature Communications* **5**, 3376 (2014).
- [36] P. Farrera, N. Maring, B. Albrecht, G. Heinze, and H. de Riedmatten, *Optica* **3**, 1019 (2016).
- [37] V. Krutyanskiy, M. Meraner, J. Schupp, and B. P. Lanyon, *Applied Physics B* **123** (2017).
- [38] M. Bock, P. Eich, S. Kucera, M. Kreis, A. Lenhard, C. Becher, and J. Eschner, *arXiv.org* (2017), 1710.04866v1.

- [39] T. Walker, K. Miyanishi, R. Ikuta, H. Takahashi, S. V. Kashanian, Y. Tsujimoto, K. Hayasaka, T. Yamamoto, N. Imoto, and M. Keller, arXiv.org (2017), 1711.09644.
- [40] A. Dréau, A. Tcheborateva, A. El Mahdaoui, C. Bonato, and R. Hanson, arXiv.org (2018), 1801.03304v1.
- [41] R. Clark, T. Kim, and J. Kim, in *2011 IEEE Photonics Society Summer Topical Meeting Series* (IEEE, 2011) pp. 45–46.
- [42] S. Wang, V. Pasiskevicius, F. Laurell, and H. Karlsson, *Optics letters* **23**, 1883 (1998).
- [43] D. B. Oh, *Optics letters* **20**, 100 (1995).
- [44] H. Rütz, K.-H. Luo, H. Suche, and C. Silberhorn, *Applied Physics B* **122**, 13 (2016).
- [45] H. Rütz, K.-H. Luo, H. Suche, and C. Silberhorn, *Phys. Rev. Applied* **7**, 024021 (2017).
- [46] Y. O. Dudin, A. G. Radnaev, R. Zhao, J. Z. Blumoff, T. A. B. Kennedy, and A. Kuzmich, *Physical Review Letters* **105**, 260502 (2010).
- [47] M. Gündoğan, P. M. Ledingham, K. Kutluer, M. Mazzera, and H. de Riedmatten, *Physical Review Letters* **114**, 230501 (2015).
- [48] O. A. Louchev, N. E. Yu, S. Kurimura, and K. Kitamura, *Applied Physics Letters* **87** (2005).
- [49] J. S. Pelc, L. Ma, C. R. Phillips, Q. Zhang, C. Langrock, O. Slattery, X. Tang, and M. M. Fejer, *Optics express* **19**, 21445 (2011).
- [50] L. Meng, A. Fix, M. Wirth, L. Høgstedt, P. Tidemand-Lichtenberg, C. Pedersen, and P. J. Rodrigo, *Optics express* **26**, 3850 (2018).